Provided for non-commercial research and education use.
Not for reproduction, distribution or commercial use.

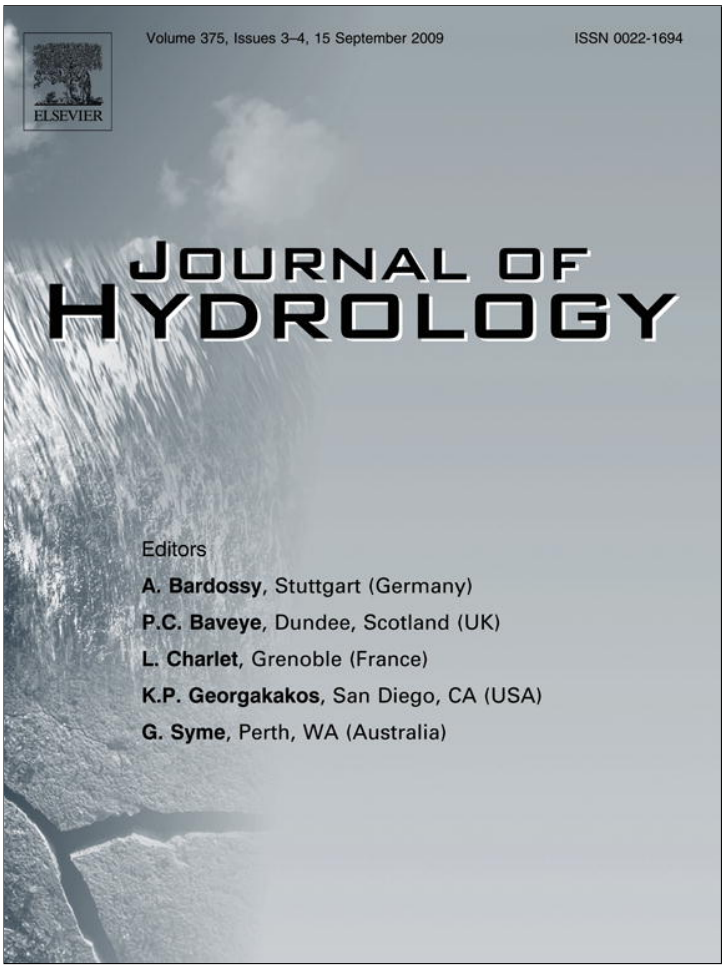

This article appeared in a journal published by Elsevier. The attached copy is furnished to the author for internal non-commercial research and education use, including for instruction at the authors institution and sharing with colleagues.

Other uses, including reproduction and distribution, or selling or licensing copies, or posting to personal, institutional or third party websites are prohibited.

In most cases authors are permitted to post their version of the article (e.g. in Word or Tex form) to their personal website or institutional repository. Authors requiring further information regarding Elsevier's archiving and manuscript policies are encouraged to visit:

http://www.elsevier.com/copyright

Author's personal copy

Journal of Hydrology 375 (2009) 513–523

Contents lists available at ScienceDirect

Journal of Hydrology

journal homepage: www.elsevier.com/locate/jhydrol

Effect of extreme rainfall events on the water resources of the Jordan River

Rana Samuels [a,*], Alon Rimmer [b], Pinhas Alpert [a]

[a] Department of Geophysics and Planetary Sciences, Faculty of Exact Sciences, Tel Aviv University, Tel Aviv 69978, Israel
[b] Israel Oceanographic and Limnological Research Ltd., The Yigal Alon Kinneret Limnological Laboratory, P.O. Box 447, Migdal 14950, Israel

ARTICLE INFO

Article history:
Received 13 November 2008
Received in revised form 23 June 2009
Accepted 1 July 2009

This manuscript was handled by P. Baveye, Editor-in-Chief

Keywords:
Extreme precipitation
Karst aquifer
Climate change
Coupled hydrological model
Jordan River

SUMMARY

As a response to climate change, shifting rainfall trends including increased multi-year droughts and an escalation in extreme rainfall events are expected in the Middle East. The purpose of this study is to evaluate the potential impact of these shifting trends on stream flow in the Jordan River and its tributaries. We use a non-homogeneous hidden Markov model to generate artificial daily rainfall simulations which capture independently shifting trends of increased droughts and escalated extreme. These simulations are then used as input into a hydrological model calibrated for the upper catchments of the Jordan River to compare the impact on stream flow and water resources between the different rainfall scenarios. We compare the predicted baseflow and surface flow components of the tested watersheds, and find that while an increase in extreme rainfall events increases the intensity and frequency of surface flow, the over all flow to the Jordan River, and the characteristics of the baseflow in the Jordan River system is not largely impacted. In addition, though it has been suggested that in the case of a multi-year drought the karstic nature of the aquifer might lead to more intense, non-linear reductions in stream flow, here we quantify and show the conditions when annual stream flow reduce linearly with rainfall, and when these relations will become non-linear.

© 2009 Elsevier B.V. All rights reserved.

Introduction

In the Middle East, recently observed trends as well as regional climate models suggest that climate change will have complex impacts on regional rainfall (Alpert et al., 2002; Krichak et al., 2007; Samuels, 2008). On the one hand, there will be less total rainfall resulting in a drier climate, while on the other an increase in the number of extreme rainfall events is expected. In Israel, most of these changes in rainfall trends will occur in the north of the country over the upper catchments of the Jordan River where reductions over the past few decades have already been recorded (Givati and Rosenfeld, 2005). These upper catchments are the main tributaries into Lake Kinneret (also known as the Sea of Galilee), an important water resource for the region. Hence, such changes are expected to cause a new distribution of runoff during the rainy season, and to lower aquifer replenishment and spring discharge, thus affecting also the other main regional water sources. Given the implications for water resource availability, there is the need to accurately model both the changes in rainfall as well as its associated impact on stream flow in the Jordan River in order to optimize future operation water policy and feasibility of interventions.

In this study, a methodology for generating artificial rainfall simulations which capture the expected changing trends is presented. The procedure for generating artificial rainfall time series based on historical trends is well established using Markov processes and neural networks (Gabriel and Neumann, 1962; Mason, 2004a). In addition, classification methods such as hidden Markov models (HMM) have proven useful for capturing hidden states ('wet' or 'dry') and reproducing daily weather patterns and rainfall statistics such as the length of dry and wet spells that are important for crop choice and agricultural decisions (Bellone et al., 2004; Thyer and Kuczera, 2000). In this study, we use a non-homogeneous hidden Markov model (NHMM) to capture the expected shift in climate trends. In NHMMs, the timing and frequency of hidden states is modified based on exogenous factors providing a way to include climatic factors or other predictors which moderate desired trends (Hughes et al., 1999a; Robertson et al., 2007, 2004; Samuels, 2008). The NHMM is used to generate rainfall simulations representing future climates which are: (1) drier and (2) more prone to extreme rainfall events. The artificial simulations are then used as input into a hydrological model to determine the impacts on stream flow, peak flow, and water recharge.

Prediction of the impact of such rainfall changes on the stream flow and river systems is not trivial. For such analysis established and well calibrated mechanisms for groundwater and stream flow recharge is needed. Here we used the Hydrological Model for Karst Environment (HYMKE, Rimmer and Salingar, 2006) for the purpose

* Corresponding author. Tel.: +972 3 6409120; mobile: +972 54 209 4300; fax: +972 3 6409282.
E-mail addresses: ranas@post.tau.co.il, rana.samuels@gmail.com (R. Samuels), alon@ocean.org.il (A. Rimmer), pinhas@post.tau.ac.il (P. Alpert).

0022-1694/$ - see front matter © 2009 Elsevier B.V. All rights reserved.
doi:10.1016/j.jhydrol.2009.07.001

Author's personal copy

of examining the effect of various rainfall patterns on the recharge of the three main sources of the Jordan River (Dan, Hermon and Snir tributaries). HYMKE is a systems approach, daily precipitation-stream flow model, which was developed for both the baseflow and the surface flow (see definitions in "Stream flow data") of large-scale karst basins. The model was applied simultaneously to these three tributaries. It was verified by comparing the calculated base flow and surface flow with daily measured data over 34 years, and demonstrated good agreement of both the surface ($r^2 > 0.6$) and base flow ($r^2 > 0.77$) components of each stream.

The sequentially coupled climate-hydrological model presented here provides a novel modeling tool for evaluating the impacts of shifting rainfall patterns due to climate change on one of the most important surface water resources in the region. The results of such a model may provide predictions for water planning and management and even for political water-related negotiations in the region.

Study area and data

The Lake Kinneret watershed

The study area in this paper is the Lake Kinneret watershed, located in the northern part of the Jordan Rift Valley (Northern Israel Fig. 1a). Lake Kinneret contributes ~30% of the Israeli water consumption. The lake water is heavily distributed through the Israeli National Water Carrier (NWC) – the national water supply system that takes water from the lake and distributes it to other parts of the country. The average area of the lake surface is 166 km^2, the average volume is 4100 Mm^3, the average annual recharge is ~400 Mm^3 and renewal period is ~10 years.

The major water source of Lake Kinneret is the upper catchments of the Jordan River (UCJR, Fig. 1b and c) with an area of ~1700 km^2. Of that area, ~920 km^2 is in Israel, and the rest is in Syria and Lebanon. The UCJR region includes four different hydrological units: (1) The Jurassic karst region of Mt. Hermon (Fig. 1b), (2) the basalt plateau of the Golan Heights, (3) the eastern Galilee Mountains, and (4) the flat alluvial Hula Valley.

An average of 480 $\times$ 10^6 m^3 of water (>80% of the entire river flow) is contributed annually (1969–2006) to the UCJR through the karstic springs and surface flow of the Mt. Hermon region (Fig. 1c), an elongated, 55-km long and 25-km wide anticline of mostly karstic limestone. Only 7% of the range lies in Israel, while the rest is divided equally between Syria and Lebanon. The Hermon high regions (above 1000 m ASL) receive the most precipitation in Israel (>1300 mm $year^{-1}$), restricted to the wet season from October to April. Precipitation on Mt. Hermon recharges the main tributaries of the upper catchments of the Jordan River (Fig. 1b): (1) Dan (255 $\times$ 10^6 m^3 annually); (2) Snir, also known as Hatzbani (118 $\times$ 10^6 m^3); and (3) Hermon, also known as Banyas (107 $\times$ 10^6 m^3).

Precipitation data

Long-term daily precipitation data from 12 stations were used. The sources of the precipitation data were the Israeli Meteorological Service (IMS). The rainfall series were compiled and corrected to prevent missing and erroneous values. Fig. 1c shows the location and the spatial distribution of the selected stations. The amount of precipitation on Mt. Hermon, was not measured systematically before 2006, because of the difficulties in maintenance of meteorological station at altitudes above 2000 m ASL (Gil'ad and Bonne, 1990). The northernmost rain gauges were located in the Golan Heights at an elevation of ~948 m ASL. Since historical records of daily rainfall intensity at the selected 12 stations vary, the years 1968–2004 were chosen for the study, given that these are the years with complete records from all 12 stations. A list of the selected station names, location, and source of the rainfall time series is shown in Table 1.

Stream flow data

The hydrological model was calibrated for default rainfall-stream flow relations using daily discharges of the main UCJR tributaries – Dan, Snir and Hermon, measured by the Israeli Hydrological Service (IHS). Stream flows were measured by continuous

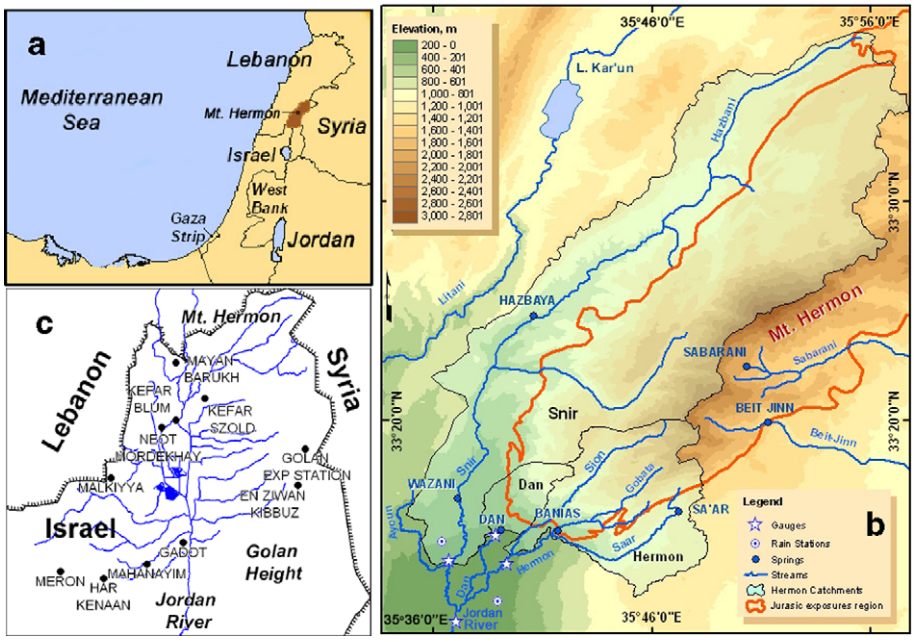

Fig. 1. (a) Orientation map of the east Mediterranean. (b) Mt. Hermon area and the Dan, Hermon, and Snir streams. (c) The upper catchments of the Jordan River with the location of rain gauges.

Author's personal copy

Table 1
Station name, longitude, latitude and altitude of selected stations.

Station	Longitude	Latitude	Altitude (m)
Mayan Barukh	35°36′	33°15′	240
Kefar Szold	35°39′	33°12′	170
Kefar Blum	35°36′	33°10′	75
Neot Mordechai	35°36′	33°09′	75
Malkiyya	35°30′	33°06′	690
Yiron	35°27′	33°04′	690
Gadot	35°37′	33°01′	100
Mahanayim	35°34′	32°59′	270
Meron	35°26′	32°59′	680
Har Kenaan	35°30′	32°58′	934
Golan experimental	35°48′	33°07′	940
Ein Ziwan	35°47′	33°05′	948

monitoring of the water level in the stream, and calibrated by periodic measurements of stream velocity profiles. The measured data were corrected for full natural flow by adding monthly consumptions. Then, stream flow time series were separated into base flow (the slow changing stream flow component, mainly originated from large karst springs) and surface flow (the quick changing stream flow component, mainly originated from small springs and surface runoff) using a procedure which was fully described and illustrated by Rimmer and Salingar (2006, see Fig. 2).

Methodology

The essence of this study is the operation of the statistical rainfall generator, and the hydrological model (Fig. 2), described herein.

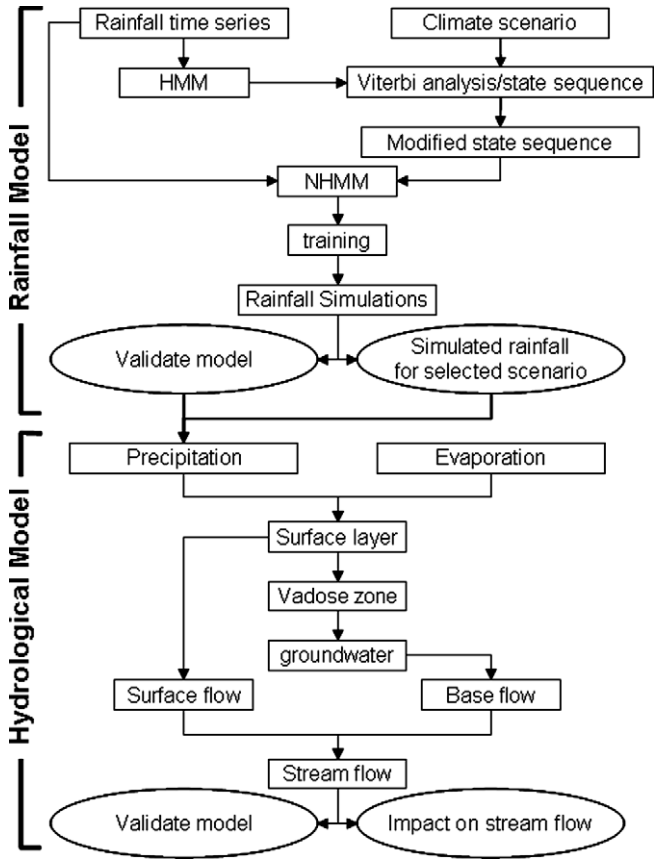

Fig. 2. Schematic of the sequentially coupled model. The top portions shows the flow of the rainfall generator while the bottom half depicts the basics of the hydrological model.

Rainfall generation

Two sets of rainfall shift scenarios were evaluated: (1) a set consistent with an increase in the number of extreme rainfall events (3-days or more) but with historical annual amounts and (2) a set consistent with a drier climate but with the historical number of annual extreme rain events. These sets were analyzed separately in order to understand their particular impact on variations in stream flow. A non-homogeneous hidden Markov model (NHMM) conditioned on varying state sequences, a vector representing the order in which one state follows the next, was used to generate the different scenarios.

Hidden Markov models

Weather generators using chain dependent markov processes have been used for decades to simulate time series of weather data (Gabriel and Neumann, 1962; Mason, 2004b; Richardson, 1981). In a Markov model, the probability that there will be rainfall on a given day R_{it} is a function of whether or not it rained the day before $P(R_{it}|R_{it-1})$ where R_{it} and R_{it-1} are the state of rainfall at station i at time t *and* $t-1$, respectively. In a hidden Markov model, the assumption is that there are different hidden states S_t (typically persistent weather regimes) each of which has its own probability of daily rainfall (and its own distribution of daily rainfall rate). The occurrence of a specific hidden state is dependant upon the state the previous day. Hence, it is the hidden states that undergo the Markovian process $P(S_t|S_{t-1})$ where S_t, refers to a general vector variable that defines an underlying weather state, which is then dependent on the previous weather state, S_{t-1}. For each day, the HMM generates rainfall simulations based on a random sampling of daily precipitation occurrences R_{it} from the probability distribution functions (pdf's) for the specific hidden state S_t (Fig. 3).

The extension of the HMM to the NHMM allows one to condition the transition from one hidden state to the next, known as the transition probabilities, on exogenous variables. In the NHMM, the dynamics of the hidden variables can then be expressed as: $P(S_t|S_{t-1}, X_t)$ where X_i is an exogenous variable vector (Fig. 3). Here the state transition matrix is treated as a (logistic) function of a multivariate predictor input time series, as described in Hughes and Guttorp (1994) and Robertson et al. (2004). In previous works, the use of exogenous climate factors from large-scale circulation patterns has improved the representation of both within season and inter-annual variability (Bellone et al., 2004; Hughes and Guttorp, 1994; Hughes et al., 1999b; Robertson et al., 2007, 2004). In this study, we use modified state sequences to generate rainfall simulations with the desired persistence and drought trends.

State sequences

Based on the state transition probability matrix from the HMM, the Viterbi algorithm (Viterbi, 1967) can be used to determine the most likely sequence of hidden states in the historical data set. Table 2 shows the transition probabilities and rainfall amount, percent of days and percent of total rainfall for each of the states in the HMM.

In the homogeneous HMM, the sequence of states and hence the occurrence and amount of rainfall is determined by the transition probabilities between the states, and the intra-seasonal and inter-annual variability is not captured. By using the viterbi, or historical state sequence as the NHMM input, we are putting back the historical intra-seasonal and inter-annual variability into the model. The rainfall simulations generated with the real viterbi sequence can be compared to historical data to evaluate the robustness of the model. Similarly, different state sequences capturing the shifting rainfall trends can be used as NHMM input to generate the desired rainfall scenarios. In this way, four distinct

Author's personal copy

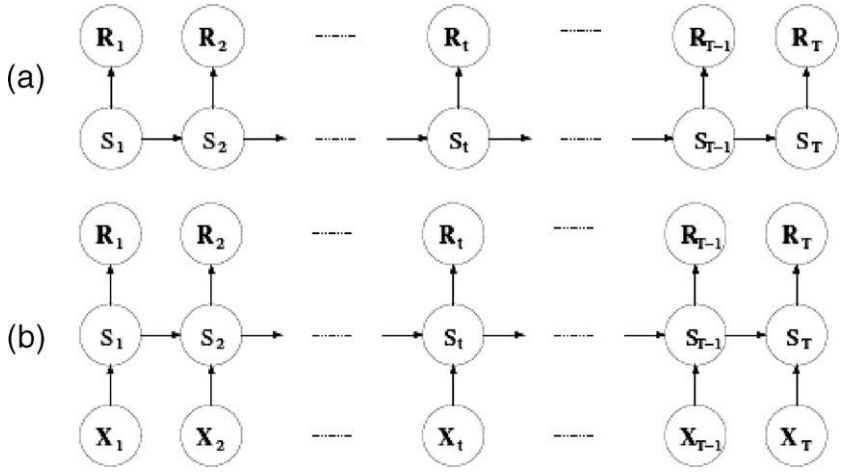

Fig. 3. Graphical model representation of: (a) hidden Markov model and (b) non-homogeneous HMM (Robertson et al. (2004)).

Table 2
(A) Transition probabilities and rainfall amount, percent of days and percent of total rainfall for historical state sequence from 4-state HMM. Transition probabilities are also used to generate baseline scenario simulations. (B) Transition probability matrix used to generate state sequence for extreme scenario. (C) Transition probability matrix used to generate state sequence for drought scenario.

A	1	2	3	4	Average amount (mm/day)	Total days (%)	Total rainfall (%)
1	0.82	0.43	0.33	0.21	0	64	0
2	0.10	0.19	0.14	0.13	0.6	12	2
3	0.07	0.25	0.27	0.23	4.6	13	19
4	0.02	0.14	0.26	0.43	22.2	11	78

B	1	2	3	4
1	0.85	0.44	0.25	0.09
2	0.06	0.25	0.27	0.16
3	0.06	0.16	0.28	0.32
4	0.03	0.14	0.20	0.43

C	1	2	3	4
1	0.93	0.42	0.22	0.06
2	0.03	0.21	0.22	0.12
3	0.03	0.21	0.33	0.34
4	0.01	0.16	0.23	0.48

groups (one validation set and three scenarios) of rainfall simulations were generated:

1. *Validation set*: NHMM input is the historical estimated state sequence as identified using the viterbi algorithm. This set of simulations is compared to the real rainfall data.
2. *Baseline scenario*: NHMM input is a state sequence generated based on historical hidden state transition probabilities. This resulted in rainfall simulations such that $R_{mean} = R_{mean\_real} \pm 5\%$ and $R_{wsc} = R_{wsc\_real} \pm 5\%$ where R_{mean} and R_{wsc} are the annual mean and number of 3 day wet spells of the simulated time series, respectively, and R_{mean_real} and R_{wsc_real} are the annual mean and number of 3 day wet spells of the historical data, respectively.
3. *Extreme scenario*: NHMM input is a state sequence generated such that $R_{mean} = R_{mean\_real} \pm 5\%$ and $R_{wsc} = R_{wsc\_real} + 25\% (\pm 5\%)$.
4. *Drought scenario*: NHMM input is a state sequence generated such that $R_{mean} = R_{mean\_real} - 25\% (\pm 5\%)$ and $R_{wsc} = R_{wsc\_real} \pm 5\%$.

For the extreme and drought scenarios, the specific state sequences were generated by modifying the transition probabilities between the different states until it resulted in rainfall simulations which met the above constraints. Then, from these new transition matrices, five state sequences were generated and each sequence was used to generate 10 NHMM simulations, resulting in 50 simulations for each group. A flow chart of the different steps can be seen in Fig. 2.

These sets of rainfall simulations were then used as input into the hydrological model. The other input of the hydrological model – daily potential evaporation – remained similar to Rimmer and Salingar (2006).

Hydrological model

The main equations for the hydrological model are part of a conceptual HYdrological Model for Karst Environment (HYMKE) (Rimmer and Salingar, 2006). In the application to the Mt. Hermon region it consists of three surface flow catchments, and four regional phreatic aquifers. HYMKE is made of four modules (Fig. 4): the surface layer (0), the vadose zone (1), groundwater (2), and surface flow (3). In the conceptual model, the land surface of the entire geographical basin is recharged by precipitation and dried by evaporation, surface runoff, and percolation to deeper layers. The karst nature of the landscape was introduced similarly to (Jeannin and Grasso, 1997), with a surface layer ("epikarst") composed of both low- and high-permeability sections that feed the karst network. The surface layer is drained continuously as a function of moisture content. Saturation excess is generated when the surface layer is

Author's personal copy

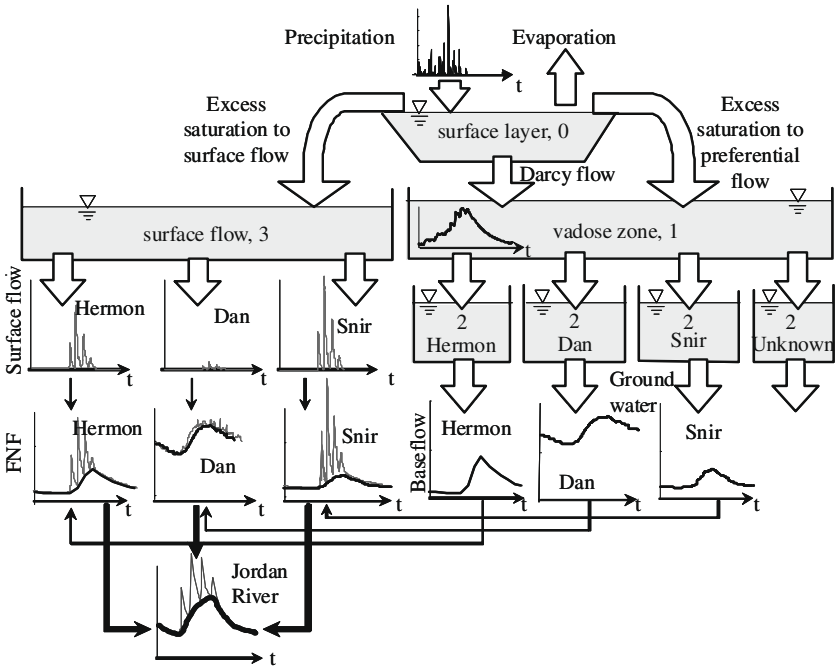

Fig. 4. Schematic description of the Mt. Hermon conceptual hydrological model: module 0 is the surface layer, module 1 is the vadoze zone, module 2 consists of four groundwater reservoirs, and module 3 simulates the surface flow. The calculated baseflow and the surface flow components of each tributary result in their full natural flow, and the combined flow creates the Jordan River.

saturated. Part of the excess saturation is then transformed into surface flow (module 3), while the other part forms a downward preferential flow component. Therefore, the percolation into the vadose zone (module 1) includes both "slow flow" component through the matrix, and "quick flow" through the high-permeability section, which is effective mainly during the peak of the wet season. The output from the vadose zone (module 1) feeds the groundwater reservoir (module 2). However, the differences between the groundwater discharge patterns require the separation of module 2 into four groundwater reservoirs. In the case of Mt. Hermon, three reservoirs feed the Dan, Snir, and Hermon baseflow component, and one reservoir contributes to the residual of groundwater to springs in the east part of Mt. Hermon in the area of Syria. The accumulating output from the surface runoff (module 3) and the baseflow (module 2) for each tributary result in the full natural flow. The sum of all three tributaries creates the flow in the main stream, the Jordan River.

Results

Rainfall simulations

The NHMM was used to make spatially disaggregated rainfall simulations for the 12 stations. Using rainfall simulations from the validation set as described in "State sequences" we compared selected statistics from the modeled rainfall with historical rainfall. Given the 36 years of data, the NHMM was trained on 30 years of data and tested on the remaining 6 years. This was repeated six times, each time leaving out a different set of 6 years. This resulted in a 36 year out-of-sample time series against which to compare the historical data and validate the model. Figs. 5a–c show the averages of the simulated results along with the 50% and 95% confidence limits compared to the observed historical data for annual amounts, 3-day wet spells and 7-day dry spells. Table 3 summarizes the correlations of the models results with the measured data for the individual stations for a range of selected statistics. For annual amounts, correlations at individual stations range from 0.56 to 0.95 with an overall correlation of 0.96. Similar correlations were found for the other selected statistics. These results suggest that the use of the estimated state sequence is a robust input for the NHMM. These simulations will also be used to validate the HYMKE hydrological model.

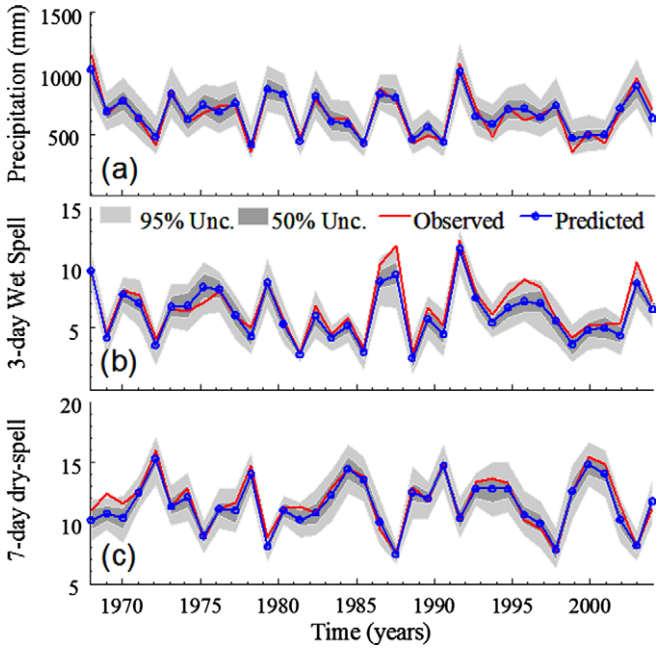

Fig. 5. (a–c): Results from 10 NHMM simulations over the period 1968–2004: (a) Precipitation amounts; (b) number of 3-day wet spells and (c) number of 7-day dry spells per season averaged across all 12 stations. Observed, simulated and 50% and 95% confidence limits are shown.

For baseline, extreme and drought scenarios, as described in "State sequences", the transition matrices for each scenario are

Author's personal copy

Table 3
Correlation of real rainfall data with model results for the 12 individual stations and for the combined total.

	Amounts	3-day wet	7-day dry	Wet days	Dry days	Wet–wet P	Dry–dry P
Mayan Barukh	0.90	0.77	0.75	0.76	0.76	0.83	0.70
Kefar Szold	0.81	0.84	0.63	0.72	0.72	0.82	0.66
Kefar Blum	0.95	0.87	0.93	0.95	0.95	0.95	0.93
Neot Mordechai	0.94	0.86	0.89	0.92	0.92	0.91	0.92
Malkiyya	0.95	0.89	0.91	0.97	0.97	0.94	0.97
Yiron	0.91	0.82	0.81	0.88	0.88	0.88	0.85
Gadot	0.73	0.77	0.40	0.48	0.48	0.64	0.39
Mahanayim	0.56	0.58	0.50	0.47	0.47	0.52	0.44
Meron	0.95	0.82	0.86	0.90	0.90	0.89	0.90
Har Kenaan	0.93	0.91	0.82	0.95	0.95	0.94	0.94
Golan experimental	0.91	0.70	0.85	0.82	0.82	0.73	0.87
Ein Ziwan	0.90	0.72	0.77	0.84	0.84	0.78	0.84
Total	**0.96**	**0.94**	**0.93**	**0.94**	**0.94**	**0.95**	**0.94**

shown in Table 2A–C. For each case we generated five different state sequences or NHMM input from the appropriate transition matrix. We then ran the NHMM model using each of these sequences 10 times resulting in 50 model runs (five sets of 10 simulations each). Table 4 shows average annual amounts, dry spell count and wet spell count from these simulations compared with the real data. From each of the five sets of 10 simulations, the set which best captured the desired new trends was chosen as input into the hydrological model.

Stream flow simulations

Application of the generated rainfall time series with HYMKE was carried out with the same procedure as described by Rimmer and Salingar (2006). A "representative" rainfall gauge of the entire Hermon region was defined and calculated from the daily generated precipitation using only four rain gauges out of the 12 stations at previous stages: Ein Ziwan, Golan Exp. Station, Malkya and Ma'ayan Barouch. These stations were chosen because a. they are the (1) most northern gauges, and (2) they represent various elevations in the northern UCJR. Therefore, the combined application of the real rainfall from these stations created a "representing" rainfall with good agreement between modeled and measured stream flows. In each simulation HYMKE created 12 time series: baseflow, surface flow and full natural flow for the Dan, Snir, Hermon and Jordan Rivers.

Validation of the combined rainfall and stream flow simulations

First, validation of the effectiveness of the model to capture stream flow was carried out, using the results of both single simulations, and the average stream flow from the set of 10 simulations from the validation set. We compare the original rainfall data with results from the validation set as well as with results from the baseline scenario. This scenario has the same average annual rainfall as well as wet and dry spells as the validation set. However, the validation set, which is based on the correct historical state sequence, captures the true inter-annual and intra-seasonal variability of the rainfall time series. In the baseline scenario, this inter-annual and intra-seasonal timing is randomized. We used three tests to check whether the integration of the artificial rainfall into the hydrological model, is valid for both baseflow and surface flow in all tributaries.

In the first test the distribution parameters (maximum – 100%, minimum – 0%, median – 50%, and the lower – 25% and upper – 75% quartiles) of each single predicted flow were compared to the best model results when the measured rainfall data were used as input, i.e. the "original model". In general a single simulation is not considered representative due to the stochastic nature of the rainfall series, and therefore averages of the multiple simulations are often used. However, such averages dampen out the peak values, so for this test, single simulations were used. Here we exemplified the distribution parameters of the calculated full natural flow in the Jordan River from a single simulation (Fig. 6a) with the same parameters from the original model (Fig. 6b). The distribution of daily stream flows using the simulations from the validation scenarios was always similar to the original model.

The second test is the r^2, where we expect that the daily predicted flows (validation set) will be in agreement with the daily measured flows. As mentioned above, given the stochastic nature of the rainfall simulations, the average of the 10 simulations from the validation set and baseline scenario were used for this test. The test was performed on each of the 12 time series. The results (Table 5) indicated that while the average of the simulations from the validation set result in lower values than the original data, they provide a much better fit than the average of the simulations from the baseline scenario, where inter-seasonal variability is randomized. This indicates that much of the seasonality is captured in the validation set. The r^2 of surface flow of the Dan River was by far less accurate than the other components of the model because it is a small component, subject to large measurement errors.

The third test is the Nash–Sutcliffe (*NS*) test (Nash and Sutcliffe, 1970), a criterion for evaluating hydrological goodness of fit between the predicted (simulated) and the measured (observed) daily values. Specifically, this test evaluates whether the model results are better ($NS > 0$), similar ($NS = 0$), or worse ($NS < 0$) than using seasonal averages. In other words, it is a measure of whether the inter-annual variability is captured. Here, (excluding the Dan surface flow) the original model resulted in $NS > 0.2$, and for most of the predicted time series $NS > 0.4$ (Table 5, "original", also Rimmer and Salingar, 2006), which indicate that this model is much better than simple seasonal averages. The results of the average predicted stream flows of the 10 simulations from the validation set, which resulted in $NS \cong 0$ (Table 5, "Validation Set"), indicated that these time series are similar to the seasonal average of the measured stream flows, and therefore the inter-annual pattern is well captured. When the same test was performed on the average simulation of the baseline scenario, it resulted in $NS < -0.5$ which, as expected, shows that the baseline scenario does not capture the inter-annual trends.

The overall conclusion from these three tests is that the artificial rainfall time series of the validation set are a good representation of the measured rainfall, capturing annual averages as well as inter-annual trends and seasonality. Their application into the hydrological model result in well understood and perfectly reasonable stream flows. This suggests that the artificially generated rainfall scenarios can be effectively used to determine the impacts of changes in rainfall trends on stream flow. Specifically, this sequen-

Author's personal copy

Table 4
Selected statistics from the rainfall simulations.

													Mean from 10 simulations	Change from real (%)
Average annual amounts														
Real	679	555	510	534	625	772	441	556	923	697	883	814	666	
Baseline scenario	692	584	534	545	651	787	458	575	944	725	912	847	688	0.03
	704	582	546	547	652	777	465	573	949	713	899	838	687	0.03
	593	501	464	467	554	674	392	492	821	635	778	723	591	−0.11
	682	570	543	535	645	776	460	563	946	721	889	822	679	0.02
	679	561	524	535	638	762	443	570	924	703	888	812	670	0.01
Increased spells	719	593	559	561	669	815	483	581	983	739	958	870	711	0.07
	657	543	516	516	611	744	429	544	883	700	874	800	651	−0.02
	616	510	471	475	562	685	395	498	816	631	801	735	600	−0.10
	701	582	545	554	656	782	466	588	970	735	920	859	696	0.05
	682	560	529	525	625	760	445	555	916	703	880	815	666	0.00
Reduced amount	501	403	380	395	447	547	330	403	667	501	641	579	483	−0.27
	490	398	380	388	456	552	327	411	673	508	638	598	485	−0.27
	482	399	371	377	453	548	326	401	663	504	623	582	477	−0.28
	521	433	402	411	489	583	351	429	704	545	671	628	514	−0.23
	506	418	392	392	462	559	330	415	682	524	644	608	494	−0.26
7-Day dry spell count														
Real	11.4	11.4	11.6	12.0	11.0	10.6	12.6	12.3	12.3	9.5	10.4	11.7	11.4	
Baseline scenario	11.3	11.5	11.5	11.9	10.7	10.5	12.8	12.3	12.5	9.3	10.3	12.0	11.4	0.00
	10.8	11.2	11.0	11.5	10.3	10.1	12.2	11.9	12.0	8.8	9.9	11.6	10.9	−0.04
	11.8	12.0	12.0	12.4	11.2	11.2	13.2	12.7	12.9	9.8	10.9	12.6	11.9	0.04
	11.3	11.5	11.5	12.0	10.8	10.7	12.6	12.2	12.5	9.4	10.4	12.1	11.4	0.00
	11.6	11.8	11.8	12.1	11.0	10.8	12.9	12.4	12.7	9.6	10.5	12.3	11.6	0.02
Increased spells	11.7	11.9	11.8	12.4	11.2	10.9	13.0	12.5	12.6	9.7	10.7	12.4	11.7	0.03
	12.0	12.2	12.3	12.6	11.5	11.3	13.2	12.9	13.1	10.1	11.1	12.8	12.1	0.06
	13.1	13.3	13.3	13.7	12.5	12.4	14.3	14.0	14.1	11.3	12.1	13.8	13.1	0.15
	11.9	12.1	12.3	12.6	11.6	11.5	13.2	12.8	13.0	10.4	11.3	12.8	12.1	0.06
	12.5	12.6	12.7	13.1	12.0	11.8	13.8	13.3	13.4	10.6	11.6	13.1	12.5	0.10
Reduced amounts	18.9	19.1	19.3	19.3	18.5	18.1	19.8	19.6	19.7	16.9	18.2	19.7	18.9	0.66
	18.7	19.0	19.2	19.2	18.4	18.0	19.5	19.3	19.5	16.9	17.9	19.5	18.7	0.65
	18.4	18.5	18.8	18.9	18.1	17.7	19.3	19.0	19.2	16.5	17.5	19.2	18.4	0.62
	18.5	18.8	19.0	19.1	18.3	17.9	19.4	19.1	19.3	16.8	17.8	19.3	18.6	0.63
	18.5	18.7	18.9	19.0	18.1	17.6	19.4	19.1	19.3	16.6	17.8	19.3	18.5	0.63
3-Day wet spell count														
Real	6.5	6.4	6.6	6.0	7.0	6.8	4.7	5.3	5.4	8.0	6.7	5.4	6.2	
Baseline scenario	6.9	7.0	7.3	6.7	7.6	7.4	5.4	6.0	6.0	8.6	7.2	6.0	6.8	0.10
	7.0	7.0	7.4	6.7	7.8	7.5	5.5	6.0	6.2	8.8	7.6	6.2	7.0	0.12
	5.9	5.8	6.0	5.4	6.4	6.2	4.5	4.8	5.0	7.2	6.2	4.9	5.7	−0.08
	7.0	7.2	7.3	6.7	7.8	7.5	5.5	6.0	6.2	8.7	7.4	6.0	6.9	0.11
	6.7	6.5	6.9	6.3	7.3	7.2	5.0	5.6	5.8	8.4	7.2	5.6	6.6	0.05
Increased spell	8.0	8.0	8.4	7.4	8.7	8.5	6.3	6.7	7.0	9.9	8.5	6.9	7.9	0.26
	7.4	7.5	7.8	7.0	8.3	7.9	5.6	6.2	6.4	9.4	7.9	6.3	7.3	0.17
	6.6	6.5	6.8	6.1	7.2	6.9	5.1	5.4	5.7	8.2	6.9	5.7	6.4	0.03
	7.9	7.9	8.2	7.5	8.6	8.3	6.2	6.6	6.8	9.8	8.3	6.8	7.7	0.24
	7.4	7.5	7.7	6.7	8.2	7.8	5.7	6.1	6.3	9.3	7.8	6.2	7.2	0.16
Reduced amount	6.0	5.9	6.2	5.6	6.4	6.3	4.7	5.1	5.3	7.2	6.2	5.1	5.8	−0.06
	5.9	6.0	6.0	5.6	6.4	6.3	4.5	5.1	5.3	7.1	6.2	5.1	5.8	−0.07
	5.8	5.7	6.0	5.4	6.2	5.9	4.4	4.7	5.0	7.0	5.9	4.9	5.6	−0.10
	6.3	6.2	6.5	6.1	6.6	6.5	5.0	5.4	5.6	7.0	6.4	5.3	6.1	−0.02
	6.4	6.4	6.6	6.0	6.9	6.6	5.0	5.4	5.5	7.5	6.5	5.5	6.2	−0.01

tially coupled climate-hydrological model can be used to evaluate the impacts of an increase in rain spells and a decrease in amounts independently. We looked at the difference in base and surface flow of the Snir and the Hermon as well as the total flow of the Jordan River under the two climate change scenarios and compared them to stream flow under current trends.

Scenarios

The simulated sets of rainfall time series were used as input into the HYMKE model. In reality, changes in rainfall affect evapotranspiration, which might also impact stream flow. However, these changes are not included in this study. Comparisons were made between the results of the baseline and the extreme and drought scenarios. Typical differences between them are demonstrated in Fig. 7, examining the soil moisture content (or the soil water storage) calculated with HYMKE during a single rainy season. Soil moisture is the single most important variable that determines the contribution of rain event to stream flow. If following rain event moisture exceeds saturation (θ_s), only then the "potential" moisture (θ_p) is transformed to surface runoff and high preferential flow recharge to groundwater. According to Fig. 7 in case 1, the soil in the extreme scenario reached saturation (and therefore contributed to stream flow) earlier during the rainy season then in the baseline scenario following higher intensity rainfall event, while in the drought scenario soil reached saturation much later during the rainy season. In case 2 the soil from the extreme scenario became drier during the season because of larger rain spells, while

Author's personal copy

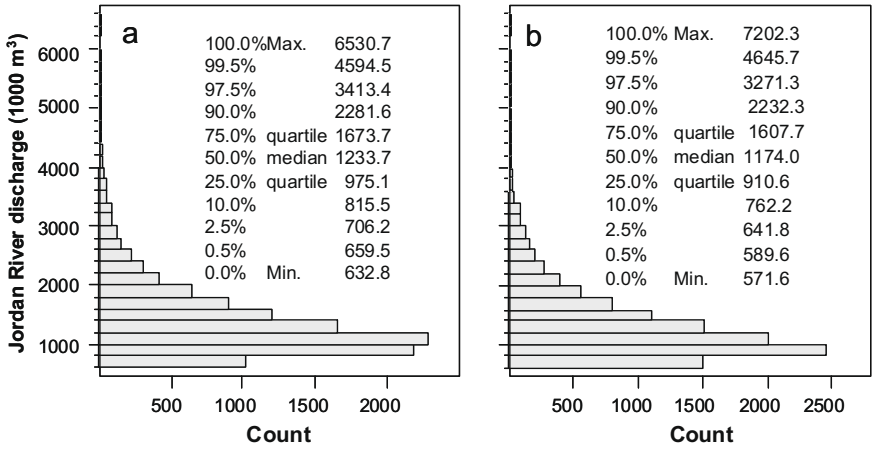

Fig. 6. Distribution of calculated full natural flow in the Jordan River: (a) Single simulation from the validation set; (b) the best model results using the measured rainfall data (original model). The largest errors in distribution parameters between validation series and original model were always smaller than ±12%.

Table 5
NS and r^2 tests for the surface, base and total flows in the Dan, Snir, Hermon and Jordan River, compared with real flow measurements during the years 1980–2000, under three scenarios: original, validation and baseline scenarios (see text for details).

1980–2000	Base flow		Surface flow		Total flow	
	NS	r^2	*NS*	r^2	*NS*	r^2
Original						
Dan	0.26	0.73	−1.55	0.44	0.21	0.68
Snir	0.69	0.84	0.46	0.62	0.55	0.69
Hermon	0.78	0.89	0.42	0.74	0.66	0.83
Jordan	0.77	0.93	0.44	0.70	0.65	0.80
Validation set						
Dan	−0.42	0.29	−0.45	0.37	−0.37	0.31
Snir	0.08	0.45	0.04	0.25	0.06	0.32
Hermon	0.11	0.54	0.04	0.38	0.10	0.48
Jordan	−0.02	0.48	0.03	0.32	0.06	0.41
Baseline scenario						
Dan	−0.98	0.04	−2.72	0.07	−1.01	0.03
Snir	−0.38	0.19	−0.85	0.02	−0.68	0.06
Hermon	−0.54	0.25	−1.31	0.06	−0.88	0.14
Jordan	−0.63	0.15	−1.19	0.04	−0.84	0.07

in the drought scenario soil was drained even more during the rainy season. In case 3, a higher rainfall event contributed larger excess saturation in the extreme than in the baseline scenario, while in the drought scenario soil was relatively dry prior to the rainfall event and therefore no excess saturation was formed.

Although there are obvious differences between the extreme and the baseline scenarios during the season, after averaging 10 scenarios, the only significant difference that remains between their results is the change in distribution of daily runoff (Fig. 8). The drought scenario, however, shows significant reduction in the overall contribution both to surface flow and base flow.

Scenario 1: increased wet spells

The results of the extreme scenario were analyzed for all the 12 stream flow time series. We found clear evidence that it will increase the probability of more intense surface flow, specifically in the Snir with the large surface area (Fig. 8a), where higher frequency of peaks above 2 million m^3/day were found (Fig. 8b). Similar changes were observed in the Hermon stream and in the cumulative surface flow in the Jordan River. However, distribution of baseflow (Fig. 8c) remained nearly similar to the baseline scenarios due to the large "damping" effect of both the vadoze zone and especially the ground water reservoirs (Fig. 4). Since ~80% of

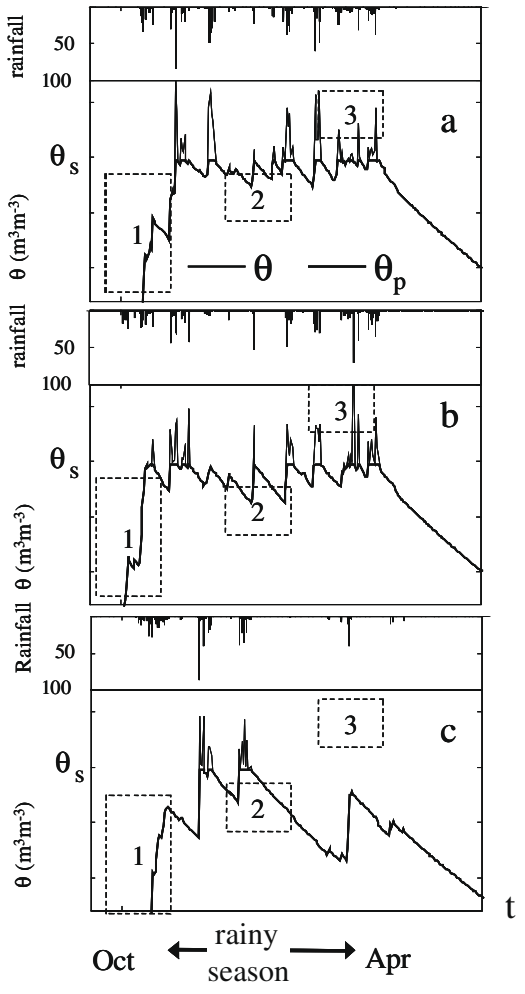

Fig. 7. Modeled soil moisture (θ) dynamics in time (t) for a single rainy season (October–April), and a single run from the baseline (a), extreme (b) and drought (c) scenarios. Daily rainfall amounts are in mm. The θ_s is soil moisture saturation and θ_p is the excess moisture that forms runoff and high recharge of groundwater. The dashed areas (1–3) demonstrate typical differences between scenarios in the tested groups (see text).

the Jordan River flow comes from karstic springs (baseflow) the effect of the change in distribution in surface flow nearly vanished from the entire Jordan River flow distribution, compared to the

Author's personal copy

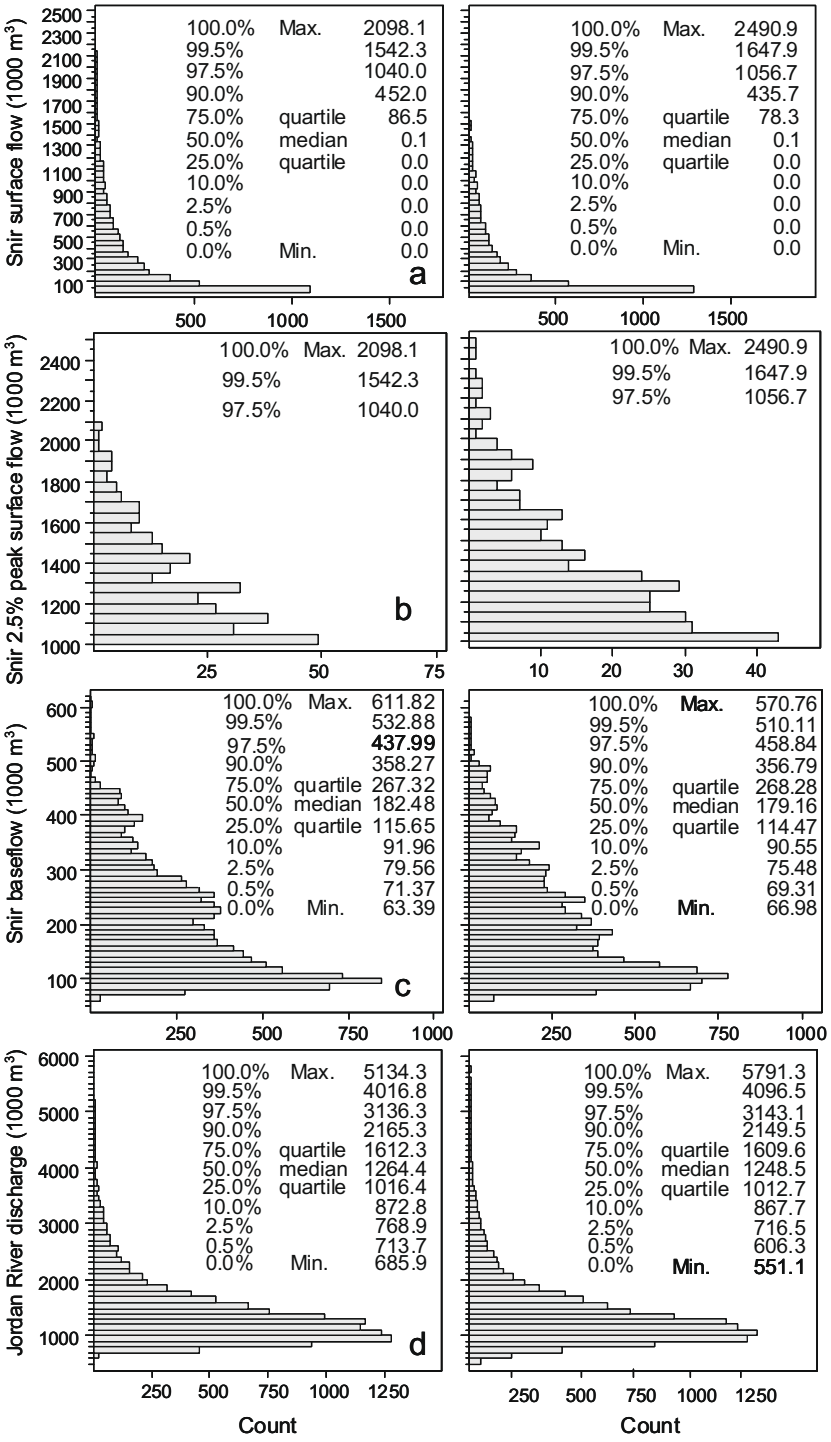

Fig. 8. Comparison of stream flow distribution with scenarios from the baseline (left) and extreme (right) scenarios: (a) surface flow in the Snir tributary; (b) distribution of the upper 2.5% of the stream flow events; (c) base flow in the Snir tributary and (d) total flow in the Jordan River.

baseline scenarios (Fig. 8d). This result indicates that more flooding is expected, however, it will not have a significant impact on the cumulative annual stream flow in the rivers analyzed as was hypothesized in the introduction.

Scenario 2: decreased amounts

The results of the drought scenario lead to a comparable reduction in the stream flow (20–25%). However, the hydrological model is not linear by definition, and the reduction in stream flow is not necessarily similar to the reduction in rainfall amounts. A typical relationship between annual surface (quick) flow and the annual rainfall (Fig. 9) reveal that at the Hermon karst as long as the annual rainfall exceeds ~400 mm, these relations are nearly linear. However if annual rainfall is less than ~400 mm (very dry year) we expect minimal additional quick flow to the rivers; a stronger reduction in the surface flow component than the reduction in rainfall amounts; and a significant deviation from the linear relations. This characteristic of the system was previously reported by Rimmer (2008).

Author's personal copy

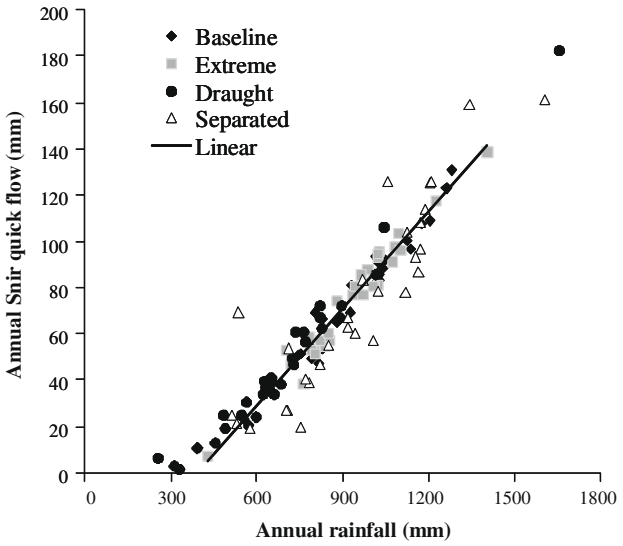

Fig. 9. Annual surface (quick) flow of the Snir River as a function of annual rainfall for the real separated data, and for the baseline, extreme and draught scenarios. The relations cease the linear relationship only if annual rainfall is less then ~400 mm annually.

Table 6
Calculated mass balance of the land surface for three scenarios.

	Baseline (%)	Extreme (%)	Drought (%)
Rainfall	100.00	100.00	100.00
Evaporation	19.41	19.14	18.64
Excess saturation	49.37	49.33	40.97
Darcy flow downward	31.50	31.83	40.92
Error	0.29	0.30	0.53

The water balances of the land surface for the three scenarios were summarized in Table 6. Evaporation depends on soil moisture, and therefore during dry conditions it was reduced in the drought scenario. A larger component of the water remaining in the land surface under unsaturated conditions is also typical of drought in karst areas, where saturation conditions were reached less often. The result is a reduction in evaporation, increased percentage of water recharging groundwater through slow Darcy flow, and an obvious reduction in the percentage of water that goes to surface flow, as well as reduced fast preferential recharge flow towards groundwater.

The expected annual flow in the Jordan River under current rainfall conditions (baseline scenario) were compared to the flows under the extreme and drought scenarios (Fig. 10). Given that the rainfall simulations are generated stochastically, there is one year (#25 in Fig. 10) where the rainfall in the drier climate is much higher than the current conditions. While the next year is again characterized by the new lower rainfall amount, the response of stream flow in the Jordan River dramatically increases in that year and then slowly decreases over the next 3 years. This is consistent with the fact that the entire Jordan River system is mainly affected by the large baseflow from the Dan Spring. The linear reservoir that represents this spring in HYMKE (Fig. 7) is known to have a recession constant of 300 days (Rimmer and Salingar, 2006), which means that the memory of this system is nearly 2–3 years. Here, by comparing this result to the real flow data in the extremely wet seasons of 1991/1992 and 2002/2003 (Rimmer, 2008), we see again that the combined system of statistically based rainfall series and hydrological model is in agreement with the real Jordan River system.

Conclusions

The question of how changes in different rainfall trends will impact stream flow is crucial for effective management and planning of river systems. The ability to assess the replenishment process of water supply systems under these scenarios is difficult as it requires both the modeling of the underlying climatic parameters as well as understanding the response of the aquifer system, neither of which is at all straightforward. The use of an integrative model which simulates rainfall with the desired characteristics as input into a hydrological model which has been shown to capture the illusive characteristics of a karst aquifer creates a tool that can effectively be used for assessing impacts of climate change and changing rainfall trends on the Jordan River System. While some of the results are expected, such as that decrease in rainfall leads to a comparable decrease in stream flow (at this level of 20–25%), some are less so. Much speculation has been made about how an in-

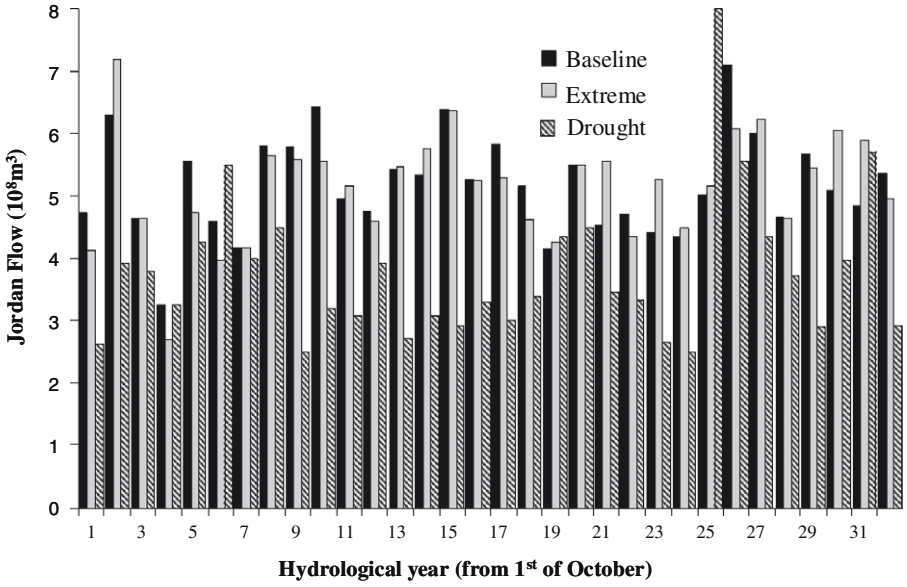

Fig. 10. Similar annual stream flow in the Jordan River for both the "baseline" and the "extreme" scenarios, and a stream flow decrease (20–25%) as a result of the reduction in annual rainfall amounts under "drought" scenario.

Author's personal copy

crease in intense rainfall trends, with more dry days, will impact the stream flow. Most of these speculations hypothesized that under such conditions the overall flow of the Jordan River will reduce, with little evidence supporting it. Here we show that while an increase in extreme rain events will results in changes in surface flow and lead to an increased risk of flooding, it will have no significant impact on total stream flow. This is due to the karstic nature of the Jordan River sources where ~80% of the flow originates from groundwater. The increased risk of flooding is especially high over the Hula Valley area with potentially destructive effects on agriculture in the region (Litaor et al., 2008). Such information about changes in rainfall regimes are important for assessing flood risk, for optimizing irrigation and agriculture and for overall integrated water management.

Acknowledgments

We would like to thank Upmanu Lall for his insightful comments and suggestions. This research was partly supported by GLOWA – Jordan River Project, funded by the German Ministry of Science and Education (BMBF), in collaboration with the Israeli Ministry of Science and Technology (MOST). The HMM code was developed by Sergey Kirshner and Padhraic Smyth, and can be obtained online at http://www.datalab.uci.edu/mvnhmm/.

References

Alpert, P., Ben-Gai, T., Baharad, A., Benjamini, E., Yekutieli, D., Colacino, M., Diodato, L., Ramis, C., Homar, V., Romero, R., Michaelides, S., Manes, A., 2002. The paradoxical increase of mediterranean extreme daily rainfall in spite of decrease in total values. Geophysical Research Letters, 29.

Bellone, E., Hughes, J.P., Guttorp, P., 2004. A hidden Markov model for downscaling synoptic atmospheric patterns to precipitation amounts. NRCSE Technical Report Series No. 021, National Research Center for Statistics and Environment, University of Washington.

Gabriel, K.R., Neumann, J., 1962. A Markov chain model for daily rainfall occurrence. Quarterly Journal of the Royal Meteorological Society 88, 90–95.

Gil'ad, D., Bonne, J.A., 1990. The snowmelt of Mt. Hermon and its contribution to the sources of the Jordan River. Journal of Hydrology 114, 1.

Givati, A., Rosenfeld, D., 2005. Separation between cloud-seeding and air-pollution effects. Journal of Applied Meteorology 44, 1298–1314.

Hughes, J.P., Guttorp, P., 1994. Incorporating spatial dependence and atmospheric data in a model of precipitation. Journal of Applied Meteorology 33 (12), 1503.

Hughes, J.P., Guttorp, P., Charles, S.P., 1999a. A non-homogeneous hidden Markov model for precipitation occurrence. Applied Statistics 48, 15.

Hughes, J.P., Guttorp, P., Charles, S.P., 1999b. A non-homogeneous hidden Markov model for precipitation occurrence. Applied Statistics 48, 15 (16 pages).

Jeannin, P.-Y., Grasso, D.A., 1997. Permeability and hydrodynamic behavior of karstic environment. In: Gunay, G., Johnson, A.I. (Eds.), Karst Waters Environmental Impact. Balkema AA, Roterdam, Netherlands, pp. 335–342.

Krichak, S.O., Alpert, P., Bassat, K., Kunin, P., 2007. The surface climatology of the eastern Mediterranean region obtained in a three-member ensemble climate change simulation experiment. Advance in Geosciences 12, 67–80.

Litaor, M.I., Eshel, G., Sade, R., Rimmer, A., Shenker, M., 2008. Hydrogeological characterization of an altered wetland. Journal of Hydrology, doi:10.1016/j.jhydrol.2007.1011.1007.

Mason, S.J., 2004a. Simulating climate over Western North America using stochastic weather generators. Climatic Change 62, 155–187.

Mason, S.J., 2004b. Simulating climate over Western North America using stochastic weather generators. Climatic Change 62 (1–3), 155–187 (33 pages Additional Info: Springer; 20040101).

Nash, J.E., Sutcliffe, J.V., 1970. River flow forecasting through conceptual models – Part 1 – A discussion of principles. Journal of Hydrology 10, 282–290.

Richardson, C.W., 1981. Stochastic simulation of daily precipitation, temperature, and solar radiation. Water Resource Research 17, 182–190.

Rimmer, A., 2008. System approach hydrology tools for the upper catchment of the Jordan River and Lake Kinneret, Israel. The Israel Journal of Earth Science 56, 1–17.

Rimmer, A., Salingar, Y., 2006. Modelling precipitation-stream flow processes in Karst basin: the case of the Jordan River sources, Israel. Journal of Hydrology 331, 524–542.

Robertson, A.W., Kirshner, S., Smyth, P., 2004. Downscaling of daily rainfall occurrence over Northeast Brazil using a hidden Markov model. Journal of Climate 17 (22), 4407–4424.

Robertson, A.W., Ines, A.V.M., Hansen, J.W., 2007. Downscaling of seasonal precipitation for crop simulation. Journal of Applied Meteorology and Climatology, 677–693.

Samuels, R., 2008. Understanding and predicting climate variations in the Middle East for sustainable water resource management. PhD Dissertation, Department of Earth and Environmental Engineering, Columbia University, New York, p. 180.

Thyer, M., Kuczera, G., 2000. Modeling long-term persistence in hydroclimatic time series using a hidden state Markov model. Water Resource Research 36, 3301–3310.

Viterbi, A.J., 1967. Error bounds for convolutional codes and an asymptotically optimum decoding algorithm. IEEE Transactions on Information Theory 13, 260–269.